Mutations in the latent TGF-beta binding protein 3 (LTBP3) gene cause brachyolmia with amelogenesis imperfecta

Mathilde Huckert, Corinne Stoetzel, Supawich Morkmued, Virginie Laugel-Haushalter, Véronique Geoffroy, Jean Muller, François Clauss, Megana Prasad, Frédéric Obry, Jean Louis Raymond, et al.

OXFORD

Human Molecular Genetics, 2015, Vol. 24, No. 11 3038–3049

doi: 10.1093/hmg/ddv053
Advance Access Publication Date: 10 February 2015
Original Article

ORIGINAL ARTICLE

Mutations in the latent TGF-beta binding protein 3 (*LTBP3*) gene cause brachyolmia with amelogenesis imperfecta

Mathilde Huckert[1,2,7,†], Corinne Stoetzel[1,†], Supawich Morkmued[2,3,11], Virginie Laugel-Haushalter[3], Véronique Geoffroy[1], Jean Muller[3,4,8], François Clauss[2,5,7], Megana K. Prasad[1], Frédéric Obry[2,7], Jean Louis Raymond[2], Marzena Switala[2,7], Yves Alembik[9], Sylvie Soskin[10], Eric Mathieu[6], Joseph Hemmerlé[6], Jean-Luc Weickert[3], Branka Brukner Dabovic[12], Daniel B. Rifkin[12], Annelies Dheedene[13], Eveline Boudin[14], Oana Caluseriu[15], Marie-Claude Cholette[15], Ross Mcleod[15], Reynaldo Antequera[16], Marie-Paule Gellé[17,18], Jean-Louis Coeuriot[17], Louis-Frédéric Jacquelin[17], Isabelle Bailleul-Forestier[19], Marie-Cécile Manière[2,7], Wim Van Hul[14], Debora Bertola[20], Pascal Dollé[3,‡], Alain Verloes[21,‡], Geert Mortier[13,14,‡], Hélène Dollfus[1,9,‡] and Agnès Bloch-Zupan[2,3,7,*]

[1]Université de Strasbourg, Laboratoire de Génétique Médicale, INSERM UMR 1112, Faculté de Médecine, FMTS, 11 rue Humann 67000 Strasbourg, France, [2]Université de Strasbourg, Faculté de Chirurgie Dentaire, 8 rue St Elisabeth, 67000 Strasbourg, France, [3]Université de Strasbourg, Institut de Génétique et de Biologie Moléculaire et Cellulaire (IGBMC), CERBM, INSERM U 964, CNRS UMR 7104, 1 rue Laurent Fries, BP 10142, Illkirch 67404, France, [4]Université de Strasbourg, Laboratoire ICube UMR 7357, CNRS, LBGI, Strasbourg, France, [5]Université de Strasbourg, Osteoarticular and Dental Regenerative NanoMedicine, Inserm UMR 1109, 11 rue Humann 67000 Strasbourg, France, [6]Université de Strasbourg, Biomaterials and Bioengineering, Inserm UMR 1121, 11 rue Humann, 67000 Strasbourg, France, [7]Hôpitaux Universitaires de Strasbourg, Pôle de Médecine et Chirurgie Bucco-Dentaires, Reference Centre for Orodental Manifestations of Rare Diseases, CRMR, 1 place de l'Hôpital, 67000 Strasbourg, France, [8]Hôpitaux Universitaires de Strasbourg, Laboratoire de Diagnostic Génétique, 1 place de l'Hôpital, 67000 Strasbourg, France, [9]Hôpitaux Universitaires de Strasbourg, Service de Génétique Médicale, 1 place de l'Hôpital, 67000 Strasbourg, France, [10]Hôpitaux Universitaires de Strasbourg, Service de Pédiatrie 1, Endocrinologie Pédiatrique, 1 place de l'Hôpital, 67000 Strasbourg, France, [11]Faculty of Dentistry, Khon Kaen

† These authors contributed equally to the work.
‡ Senior authors.

Received: November 15, 2014. **Revised and Accepted:** February 6, 2015

University, Khon Kaen, Thailand, [12]Department of Cell Biology, NYU Langone Medical Centre, New York, USA, [13]Center for Medical Genetics, Ghent University, Ghent University Hospital, De Pintelaan 185, Ghent 9000, Belgium, [14]Department of Medical Genetics, University of Antwerp and Antwerp University Hospital, Prins Boudewijnlaan 43, Edegem 2650, Belgium, [15]Department of Medical Genetics, Faculty of Medicine and Dentistry, University of Calgary, Alberta Children's Hospital, Calgary, AB, Canada, [16]Dentistry Division, HC/FMUSP, São Paulo, Brazil, [17]Faculté d'Odontologie, Université de Reims Champagne-Ardenne, 2 rue du Général Koenig, Reims 51100, France, [18]Laboratoire EA 4691 'BIOS', 1, rue du Maréchal Juin, Reims 51100, France, [19]Faculty of Dentistry, Paul Sabatier University, LU51, Pôle Odontologie, Hôpitaux de Toulouse, 3 Chemin des Maraîchers, Toulouse, France, [20]Unidade de Genética do Instituto da Criança, Hospital das Clínicas da Faculdade de Medicina da Universidade de São Paulo – Instituto de Biociências, Universidade de São Paulo, São Paulo, Brazil and [21]Département de Génétique – Hôpital Robert Debré, CRMR 'Anomalies du Développement & Syndromes Malformatifs', CRMR 'Déficiences Intellectuelles de Causes Rares', 48 bd Sérurier, Paris 75019, France

*To whom correspondence should be addressed at: Faculty of Dentistry, University of Strasbourg, 8 rue St Elisabeth, 67000 Strasbourg, France. Tel: +33 368853919; Fax: +33 368853900; Email: agnes.bloch-zupan@unistra.fr

Abstract

Inherited dental malformations constitute a clinically and genetically heterogeneous group of disorders. Here, we report on four families, three of them consanguineous, with an identical phenotype, characterized by significant short stature with brachyolmia and hypoplastic amelogenesis imperfecta (AI) with almost absent enamel. This phenotype was first described in 1996 by Verloes *et al.* as an autosomal recessive form of brachyolmia associated with AI. Whole-exome sequencing resulted in the identification of recessive hypomorphic mutations including deletion, nonsense and splice mutations, in the *LTBP3* gene, which is involved in the TGF-beta signaling pathway. We further investigated gene expression during mouse development and tooth formation. Differentiated ameloblasts synthesizing enamel matrix proteins and odontoblasts expressed the gene. Study of an available knockout mouse model showed that the mutant mice displayed very thin to absent enamel in both incisors and molars, hereby recapitulating the AI phenotype in the human disorder.

Introduction

Brachyolmia (from the greek 'short trunk') refers to a heterogeneous group of skeletal dysplasias with as major clinical feature a disproportionate short stature with short trunk. Radiographic abnormalities are predominantly present in the axial skeleton and include generalized platyspondyly (i.e. flattened vertebral bodies). Amelogenesis imperfecta (AI) is a defect in enamel formation and mineralization (1). AI can be an isolated finding or occur in association with other anomalies (syndromic AI) (2). In 1996, Verloes *et al.* (3) described an autosomal recessive form of platyspondyly with AI [MIM 601216]. Absence of enamel and oligodontia were the major dental findings. Bertola *et al.* (4) subsequently published two other families, one of them with abnormal yellow coloration of primary and permanent teeth, as well as retarded dental eruption compatible with a diagnosis of AI. Here we report on four families, three of them being consanguineous, with an identical phenotype, characterized by platyspondyly (brachyolmia) and AI. Affected individuals have very thin or almost absent enamel. By using a combined strategy of homozygosity mapping and whole-exome sequencing, recessive mutations in the latent TGF-beta binding protein 3 (*LTBP3*) gene were identified. Analysis of *ltbp3* expression during mouse development and the study of dental anomalies observed in the *Ltbp3*$^{-/-}$ knockout mouse model underscored the key role of the latent TGF-beta binding protein 3 in amelogenesis and skeletal development.

Results

Patients' phenotype

The index family 1 presented with AI and short stature. The almost complete absence of enamel in both primary and permanent dentitions (Fig. 1A and B) led to the diagnosis of hypoplastic AI, thereby explaining the yellow, small and spaced appearance of the teeth. The panoramic radiographs confirmed the absence of enamel associated with large pulp chambers and taurodontic molars (Fig. 1C). Class III mandibular prognathism encountered in family 1 was due to maxillary underdevelopment (Fig. 1D). Radiographs of the skeleton revealed brachyolmia (Fig. 1E and F)

Subsequently, three additional families with a similar phenotype were identified. Additional bone anomalies such as osteopenia and scoliosis were present in family 4. Missing teeth (family 4) and retarded teeth eruption (family 3) were also reported.

Enamel shows quantitative and qualitative defects

The enamel structure of a permanent tooth, the left upper second premolar (25) extracted within the course of treatment of patient IV-1 of family 1 was further analyzed by scanning electron microscopy (Fig. 1G and H). With this evaluation the enamel hypoplasia was confirmed and very thin or absent enamel was noted. Dentin was normal. The initial aprismatic enamel layer was absent. A very thin shell of irregular prismatic enamel (PE), with a reduced thickness thinner than 150 µm (instead of 300 µm comparatively at the same site on a control tooth), was deposited covering the dentin scaffold. In this layer, a Hunter-Schreger band pattern, featuring the arrangement of enamel prisms, was present. In these areas, no aprismatic outer layer was deposited. However in some areas, amelogenesis continued and some 'bubbling' of non-prismatic enamel (NPE) occurred on top of this basal first enamel layer. Waves of aprismatic and prismatic enamel alternated. The outermost layer was always aprismatic in areas where enamel formation continued.

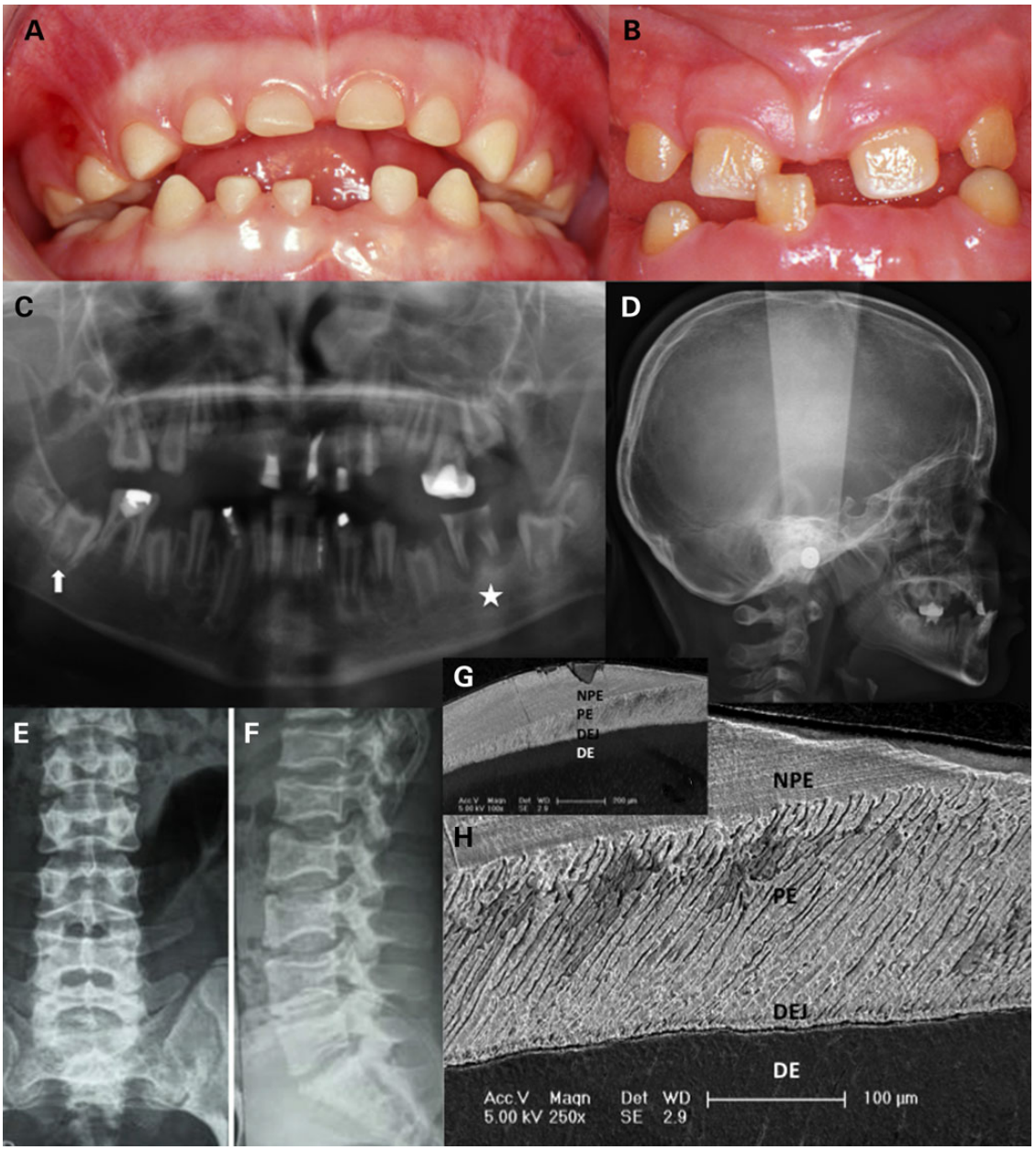

Figure 1. Phenotypic data on family 1. (**A**) Intraoral view of individual IV.1 (at age 5 years). All primary teeth are smaller and yellowish showing thin, almost absent, enamel. The dentition is spaced. (**B**) Intraoral view of individual IV.2 (at age 7 years). The erupting permanent incisors are yellow and small due to absent enamel. Primary teeth were lost after recurrent infections. (**C**) Panoramic radiograph of individual IV.2 (at age 9 years) showing erupted and non-erupted permanent teeth with no enamel. No teeth are missing. Pulp chambers appear large. Infection as a consequence of microbial contamination of pulp spaces is visible around the 36 (radiolucent area around the roots of the lower left first permanent molar filled star) in the absence of the protective enamel layer. The upward arrow points toward a second right lower permanent molar not yet erupted presenting with taurodontism and a large pulp chamber. (**D–F**) Radiographs taken from individual IV.2 (skull at age 9 years and spine at age 14 years). Skull radiograph reveals absent pneumatization of sinuses and mandibular prognathism secondary to underdevelopment of the maxilla. The spine radiographs show platyspondyly with indentations of both upper and lower vertebral endplates. (**G**) The enamel phenotype analyzed at the ultra-structural level through SEM revealed a thin PE layer directly starting at the dentino-enamel junction (DEJ). In some areas enamel formation continued as an aprismatic layer (NPE). Dentin (DE) was normal. (**H**) Close up of the PE and NPE thin layer.

Mutations in *LTBP3* underlie syndromic AI with brachyolmia

Whole-exome sequencing was performed independently (in two different labs) in families 1 and 2 and in families 3 and 4. Coverage and variant calling data for families 1 and 2 are provided in Supplementary Material, Table S1.

A single gene, *LTBP3*, was found to carry bi-allelic mutations in all affected individuals from the four families (Fig. 2A and B). In family 1, we identified a homozygous 14 bp deletion, c.[2071_2084delTACCGGCTCAAAGC] (Table 1 and Fig. 2A). This mutation lies within a zone of homozygosity that is shared between the two affected individuals, but that is absent in the unaffected sibling and parents (Supplementary Material, Fig. S1).

In family 2 we identified compound heterozygosity for a nonsense and a splice donor site mutation c.[421C>T];[1531+1G>T]; in families 3 and 4 homozygosity for a single nucleotide deletion was found (c.[2216_2217delG] in family 3 and c.[2356_2357delG]

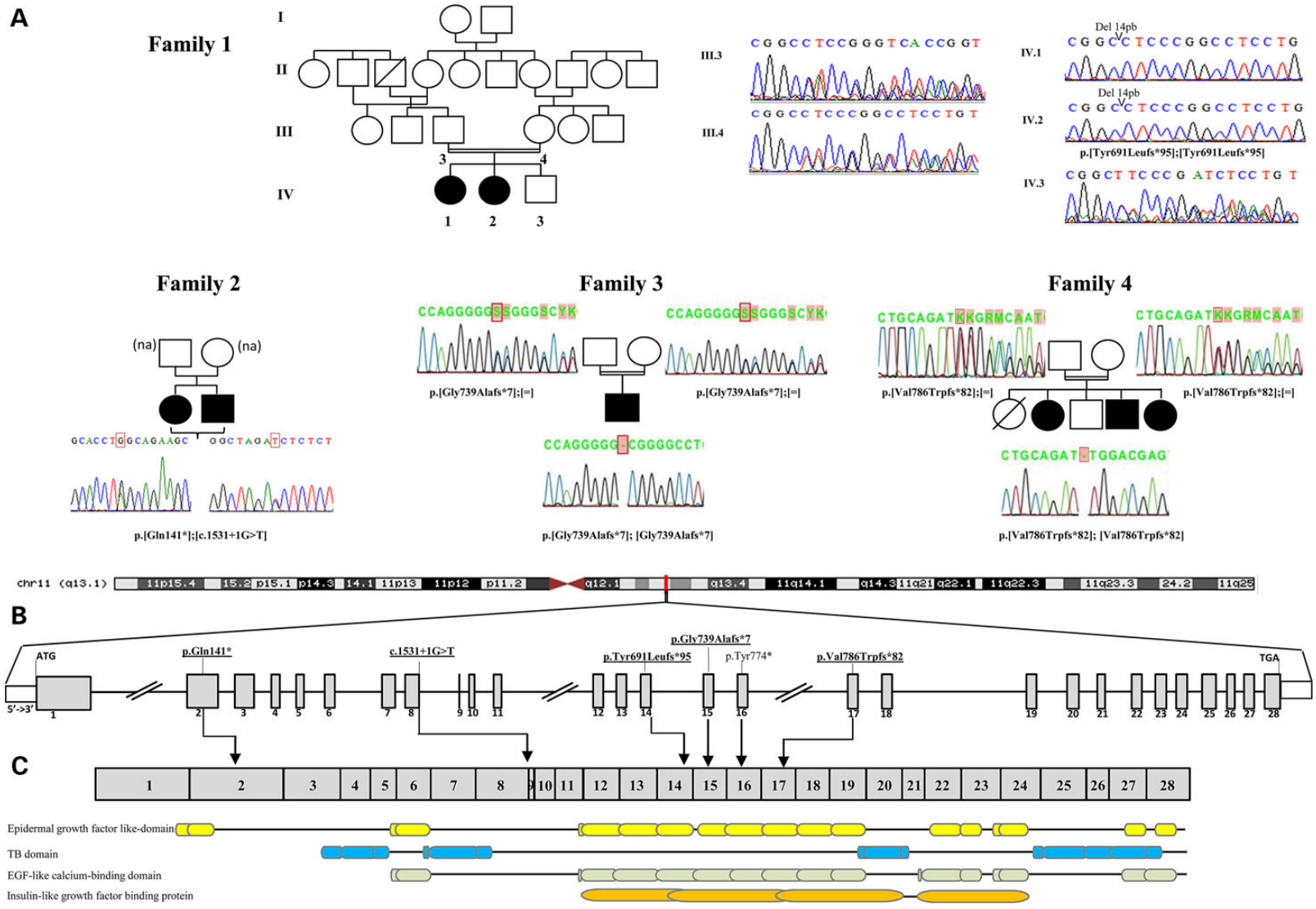

Figure 2. Detected *LTBP3* mutations and corresponding protein domains. (**A**) Pedigrees and sequences analysis of families 1–4 (na: not available). Simplified pedigree of family 1 demonstrates consanguinity between the parents III.3 and III.4. Electropherograms reveal a 14-bp homozygous deletion in the affected individuals IV.1 and IV.2. The parents III.3 and III.4 are heterozygous for the deletion. (**B**) The *LTBP3* human gene is located on chr11q13.1, extends over 20 kb and contains 28 exons (vertical gray hatches); the position of the start codon (ATG) and the stop codon (TGA) are indicated. The mutations detected in this study are bold and underlined, vertical lines indicate positions relative to exons (only the p.Tyr774* was previously described in Noor *et al.* (5)). (**C**) Arrows indicate positions relative to the cDNA and the protein domain according to EMBL-EBI Interpro.

Table 1. Mutations described in LTBP3 (NM_001130144.2)

Family	Affected	Ethnic origin	#Exon	Chromosomic position (hg19)	cDNA change	Protein change
1	Two siblings	Turkey	Exon 14	g.65314933	c.[2071_2084delTACCGGCTCAAAGC]; [2071_2084delTACCGGCTCAAAGC]	p.[Tyr691Leufs*95]; [Tyr691Leufs*95]
2	Two siblings	Caucasian French	Exon 2 and 8	g.65321762	c.[421C>T(;)*1531*+1G>T]	p.[Gln141*(;)?]
3	One boy	Brazil	Exon 15	g.65314283	c.[2216_2217delG]; [2216_2217delG]	p.[Gly739Alafs*7]; [Gly739Alafs*7]
4	Three siblings	Pakistan	Exon 17	g.65311018	c.[2356_2357delG]; [2356_2357delG]	p.[Val786Trpfs*82]; [Val786fs*82]

Mutation affecting splice are in *italics*.

in family 4). All mutations segregated with the disease phenotype in each family and were confirmed by Sanger sequencing (Fig. 2). In addition, they were absent in the Exome Variant Server (EVS) and the Thousand Genomes Project Catalog. Interestingly a single nucleotide insertion (c.2216_2217insG; p.Gly740Argfs*51) was tabulated in EVS in the homozygous state in 7 out of more than 6098 individuals. However, coverage information was not available for these individuals to verify if this is a false or true positive variant.

The *LTBP3* mutations identified in our families are most likely hypomorphic. The 14-bp deletion found in family 1 does not seem to result in nonsense-mediated decay because it was present in RNA extracted from a gingival biopsy of patient IV.1 (Supplementary Material, Fig. S2). The mutation most likely gives rise to a truncated protein that lacks the terminal 612 amino acids, which encode essential functional domains (epidermal growth factor like-domain, TB domain, EGF-like calcium-binding domain and insulin-like growth factor binding protein domain) of the protein (Fig. 2C). The splice-site mutation in family 2 is predicted to cause an in-frame skipping of exon 8. The remaining mutations, one nonsense mutation and two single nucleotide deletions, are expected to result in nonsense-mediated decay through the creation of a premature stop codon.

Expression pattern of *Ltbp3* in developing mouse bone and tooth

To gain insight into *Ltpb3* expression during bone and tooth development in mice, we performed an *in situ* hybridization analysis, using a digoxigenin-labeled antisense riboprobe generated from the same DNA template as previously used by the EURExpress consortium (www.eurexpress.org). Mouse embryos were analyzed at E14.5, E16.5 and E18.5. *Ltbp3* transcripts were detected in several developing tissues and organs. Expression was found in various developing bones undergoing either endochondral or intramembranous ossification (e.g. the vertebrae: Fig. 3A; mandibular bone: Fig. 3B; base of the skull bones: Fig. 3C). Expression was also detected in the ventricular and subventricular zones of the developing brain vesicles (Fig. 3D), and in cells surrounding the lumen of the neural tube (the spinal cord primordium: Fig. 3A). Discrete expression was observed in the developing inner ear (cochlea: Fig. 3C). *Ltbp3* transcripts were detected in the small and large intestine, with most conspicuous expression at the base of the intestinal crypts (Fig. 3E). Weaker expression was seen in the differentiating lung (Fig. 3F), whereas discrete expression was observed in the heart outflow tract (not shown) and in the wall of the large blood vessels such as the aorta and pulmonary artery (Fig. 3F).

Ltbp3 expression pattern was also investigated during tooth development. In a large-scale gene expression study (www.eurexpress.org), *Ltbp3* transcripts were detected at E14.5 cap stage of tooth development (6). This also has been documented in a mouse tooth cap stage transcriptome analysis (6). Our analysis confirmed these data. In addition we investigated more precisely *Ltbp3* expression at various stages of tooth development (Fig. 3G, I and K lower incisor and H, J and L molar). *Ltbp3* transcripts were observed at E14.5 in cap stage teeth, at E16.5 in the epithelial and mesenchymal compartments of the bell stage teeth, especially in the most differentiated areas such as the molar cusp tips and the rostral part of the incisors. At E18.5 labeling was observed in differentiating ameloblasts and odontoblasts. Transcripts were scattered at the apical secretory pole of ameloblasts.

Ltbp3$^{-/-}$ mouse dental phenotype

We further explored the dental phenotype of *Ltbp3*$^{-/-}$ mice described in (7–9) by X-ray micro-computed tomography (microCT) and histological analysis to compare morphological phenotype in mouse (10) and human. *Ltbp3*$^{-/-}$ mutant mice displayed enamel defects with very thin to absent enamel in both incisors and molars (Fig. 4). Hence, the *Ltbp3*$^{-/-}$ mouse model clearly recapitulates the AI phenotype observed in our patients. Mandibular relative class III prognathism due to maxillary underdevelopment, seen in patients IV.1 and IV.2 of family 1, was also present in the mutant mouse model. Histological analysis of continuously growing incisor enamel organ revealed a cohesive, however at defined localizations, non-palisadic ameloblasts layer facing a thinner disorganized enamel matrix (Fig. 4M) confirming at the cellular level the dysfunction of amelogenesis.

Discussion

Using a combined strategy of homozygosity mapping and whole-exome sequencing in four unrelated families with the association of brachyolmia and AI, we identified the *LTBP3* (latent TGF-beta binding protein 3) gene as the underlying causal gene responsible for this rare autosomal recessive disorder [MIM 601 216]. Mutations in the *LTBP3* gene have already been reported in individuals with oligodontia (5), a dental developmental disorder defined by the absence of more than six permanent teeth. The question therefore arises if mutations in *LTPB3* can cause different dental phenotypes and how we can explain the presence of extra-dental manifestations such as brachyolmia in our families.

One gene associated with different phenotypes?

A homozygous nonsense mutation in the *LTBP3* gene was first reported in a consanguineous Pakistani family with oligodontia (5).

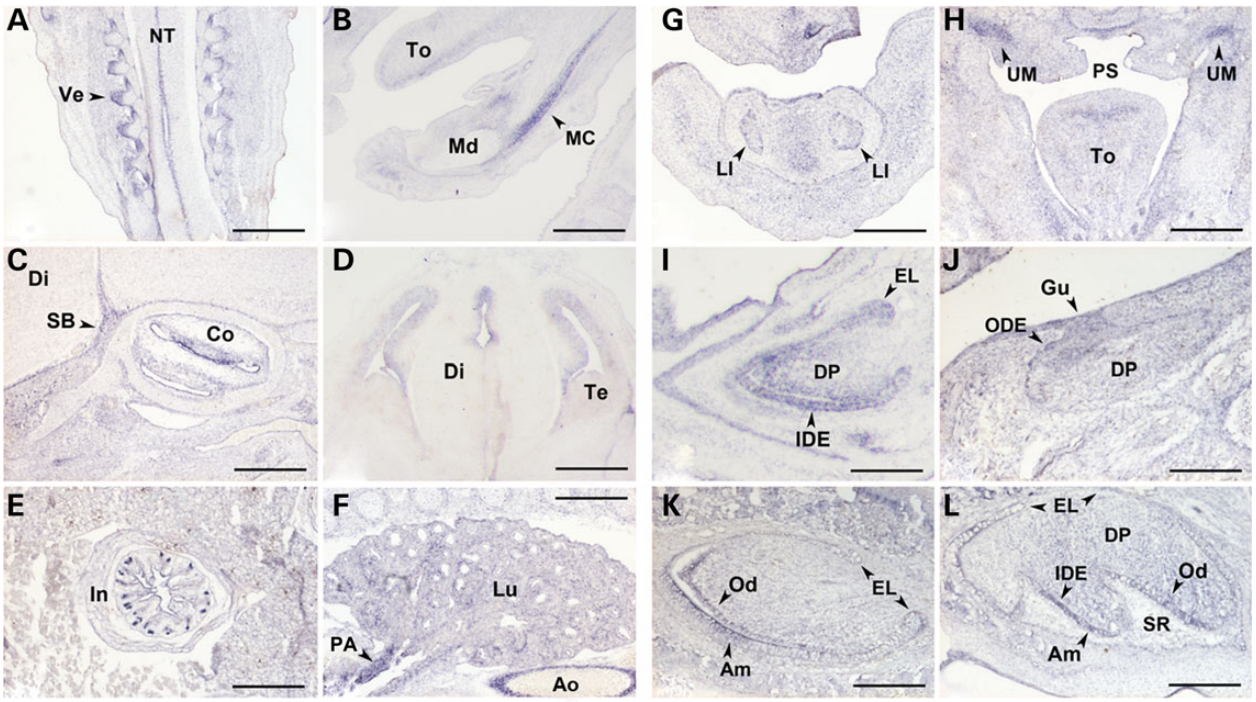

Figure 3. Analysis of mouse *Ltbp3* transcripts distribution by *in situ* hybridization. Selected sections illustrating *Ltbp3* expression features in the developing bone, central nervous system and viscera are shown in the left-side panels (**A–F**), whereas right-side panels focus on incisor (**G**, **I** and **K**) and molar (**H**, **J** and **L**) tooth development. Developmental stages and section planes are: E14.5 frontal (A, D, F, G and H), E16.5 sagittal (B, C, I and J); E18.5 sagittal (E, K and L) sections. Am, ameloblasts; Ao, aorta; Co, cochlea; Di, diencephalon; DP, dental papilla; EL, epithelial loop; Gu, gubernaculum; IDE, inner dental epithelium; In, intestine (duodenum); LI, lower incisor; Lu, lung; MC, Meckel's cartilage; Md, mandible; NT, neural tube; Od, odontoblasts; ODE, outer dental epithelium; PA, pulmonary artery; PS, palatal shelves; SB, skull bone; SR, stellate reticulum; Te, telencephalon; To, tongue; UM, upper molar; Ve, vertebrae. Scale bars: 40 µm (B and D–H); 50 µm (C, K and L); 80 µm (I and J); 150 µm (A).

Based on the available data in the report, we believe that the oligodontia phenotype in this family was either related to early loss of teeth due to enamel defects or caused by defective tooth development leading to absent teeth. Close examination of the skull X-ray of an affected patient in their published Figure 2 (5) clearly shows absent enamel and short roots in the remaining teeth, which suggests the diagnosis of an AI. Verloes *et al.* also mentioned oligodontia as a feature in his family with brachyolmia and AI (3). Missing teeth were also found in our family 4. Oligodontia may therefore be part of the clinical spectrum of this condition. The affected individuals in the consanguineous Pakistani family with oligodontia also presented with short stature. Varying degrees of scoliosis were apparently present but no other skeletal anomalies were observed. The authors do not report flattening of the vertebral bodies in their family and no lateral views of the spine are shown in their article. They only describe a higher bone mineral density in the spine found by dual-energy X-ray absorptiometry. Although we cannot judge on the presence or absence of brachyolmia as cause of the short stature in the affected individuals, we believe that this reported family with oligodontia may be affected by the same disorder given the presence of a recessive mutation in the *LTBP3* gene.

LTBP3 and TGF-beta acting as partners

The *LTBP3* gene (NM_001130144.2, 11q13.1) spans 28 exons, has 20 372 base pairs and generates 22 different transcripts (only two major transcripts with CCDS number, eight without a protein and two resulting in nonsense-mediated decay).

LTBP3 codes for a protein of the extracellular matrix that is involved in regulation of TGF-beta secretion, trapping and activation (11–13). LTBP3 (1139 amino acids, NCBI RefSeq: NP_001157738.1; 1303 amino acids NM_001130144.2) is one of the four members of the LTBP/fibrillin family and can form a large complex with latent TGF-beta 1, 2 and 3 (14). The LTBP protein domain structure consists of EGF-like calcium-binding conserved domains, 4 TGF-beta-binding protein-like (TB) domains also named eight cysteine repeats as well as insulin-like growth factor binding protein domains (Fig. 2). This domain structure is also found in TGF-binding protein and fibrillins.

LTBP3 and AI

TGF-beta 1, 2 and 3 are growth factors involved in various biological functions such as cell growth and differentiation, extracellular matrix secretion and remodeling. TGF-beta signaling is essential for hair and tooth growth especially enamel formation. Enamel is a complex structure secreted by ameloblasts presenting different successive stages during their life cycle. In mammals it is possible to recognize an initial aprismatic enamel layer at the dentin–enamel junction deposited by secreting ameloblasts without Tomes' process, then the bulk of enamel with rod and interrod compartments forms with secreting ameloblasts with Tomes' process and finally the last-formed surface aprismatic layer of enamel with the retraction of ameloblasts' Tomes' process (15). *Ltbp3* expression pattern in differentiating ameloblasts and odontoblasts is highly similar to that of *TGF-beta1* (16–18). Blockade of TGF-beta signaling results in a failure of ameloblasts to produce an enamel layer in incisor teeth (11). Overexpression of TGF-beta1 in teeth results in detachment of ameloblasts and enamel defects (1,19). *TGF-beta1* and *TGF-beta receptor 1 (TGFBR1)* genes are strongly expressed in secreting

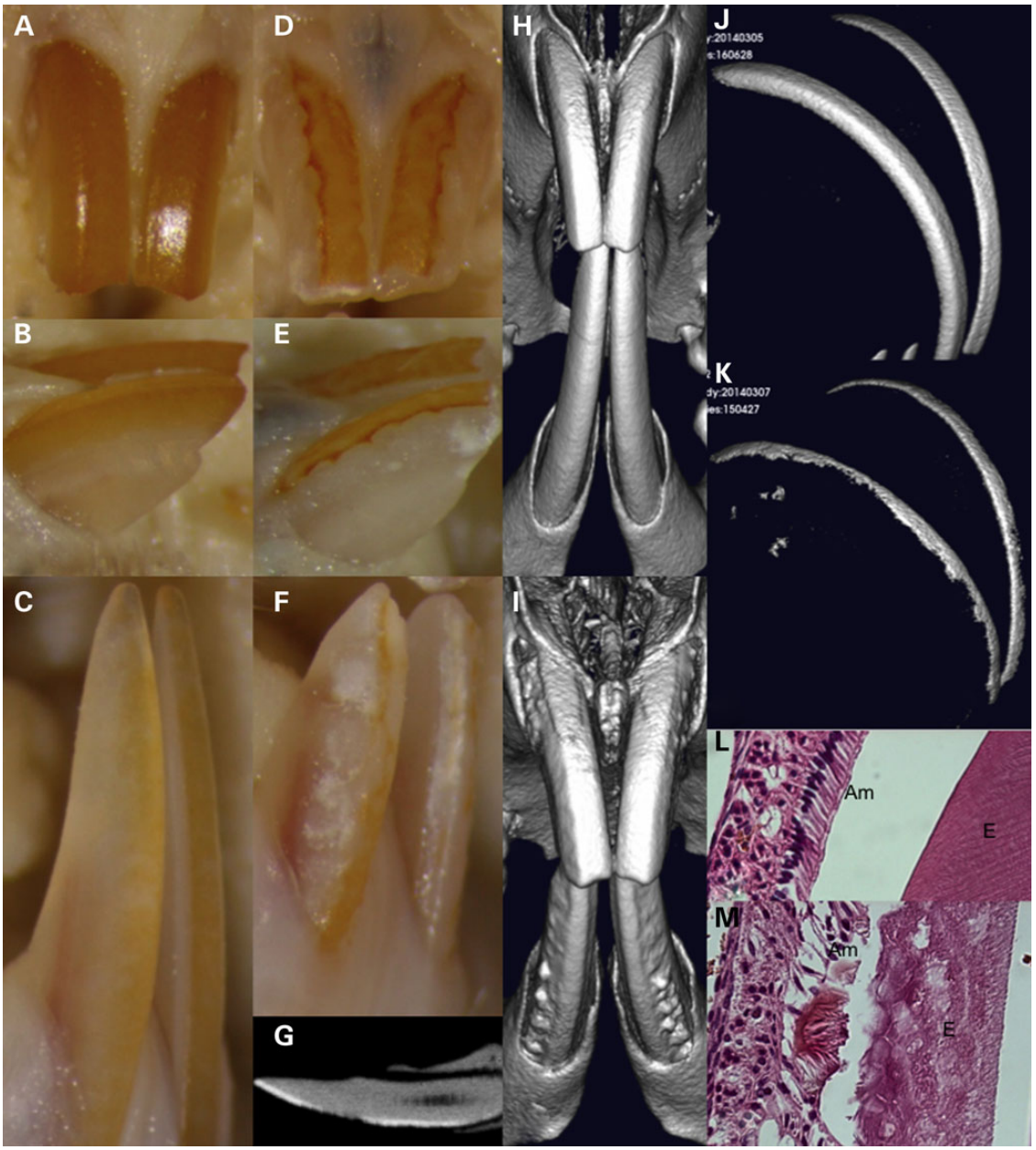

Figure 4. MicroCT and histological analysis of *Ltbp3*$^{-/-}$ mice. The Quantum FX® microCT Pre-clinical In Vivo Imaging System is a low X-ray dose system devised for longitudinal microCT in preclinical studies (Caliper Life Sciences, Inc., Hopkinton, MA, USA). Seven *Ltbp3*$^{-/-}$ mouse heads and seven WT littermates were analyzed. (**A–C**) Normal macroscopic aspect of the mouse upper (A face, B side view) and lower incisors (C: side view). Note that the teeth are naturally colored yellow that enamel is smooth and present only on the labial side. The lower incisors are twice as long as the upper. (**D–F**) Enamel defects encountered in *Ltbp3*$^{-/-}$ mouse. The colored area is decreased and an irregular indented enamel surface is present. (**G**) Appearance of lower incisor from *Ltbp3*$^{-/-}$ mouse as observed by X-ray imaging. Note irregular contour of thin enamel, a hypoplastic area, with limited or no enamel is seen on the labial side. (**H–I**) 3D reconstruction of microCT imaging demonstrating the outer surface appearance and contact between continuously growing incisors in a WT mouse (H) or *Ltbp3*$^{-/-}$ mouse (I). The enamel surface is reduced and the tooth surface irregular. (**J–K**) Normal (J: WT) and reduced (in size and density) enamel layer (K: *Ltbp3*$^{-/-}$ mouse), as observed when isolated from dentin through its highest mineralization and therefore X-ray density degree. (**L**) Normal ameloblasts (Am) layer facing a highly organized decalcified enamel (E) matrix. (**M**) In the *Ltbp3*$^{-/-}$ mouse, in certain area, the ameloblast layer became erratic, like blubbing and laid out a differently organized thinner enamel matrix.

ameloblasts where they promote the expression of *MMP20*, an enamel matrix protease (20). TGF-beta1 is also expressed later in the maturation-stage ameloblasts and seems to play an important role in ameloblast apoptosis (21). In addition, TGF-β1 is able to induce *KLK4* (a protease degrading enamel proteins to increase mineralization) expression (22,23). TGF-beta1 may also control cell layer integrity for odontoblasts (24).

The enamel defects, observed in our families, at the ultrastructural level (Fig. 1) with both the absence of the initial aprismatic enamel layer and the abnormal secretion of non-prismatic bulk enamel, strongly suggest a role of LTBP3 during the life cycle of ameloblasts especially at the secretory stages with Tomes process formation/modulation. The molecular mechanisms that control the formation, function and retraction of Tomes' process

are not well understood. However clear molecular differences exist between NPE and PE (25) and this may involve TGF-beta signaling. Transgenic mice presenting with enamel defects such as the amelotin (AMTN) overexpression model also exhibit enamel defects in relation with the disappearance of Tomes' process (26). We therefore formulate the hypothesis that TGF-beta signaling is involved in the modulation of Tomes' process and the deposition of a decussating prisms enamel pattern. Interestingly, the *Klk4* ablated mice display rod/interod anomalies besides enamel maturation defects (27).

LTBP3 and brachyolmia

LTBP3 is also involved in bone formation and remodeling. Inactivation of *LTBP3* reduces TGF-beta activation and therefore diminishes associated cell proliferation and osteogenic differentiation (28). TGF-beta is the most abundant growth factor in bone playing a major role in bone development and skeletogenesis, especially during endochondral ossification but also later in adult bone homeostasis and remodeling (29). Deregulation of the TGF-beta signaling pathway is likely to interfere with axial skeleton patterning (30).

Ltbp3 is expressed in cartilage primordia especially in developing vertebrae (7). Recently, genes such as *TRPV4* (transient receptor potential cation channel, subfamily V, member 4 gene) have been identified in autosomal dominant brachyolmia (31) and *PAPSS2* (3′-phosphoadenosine 5′-phosphosulfate synthase 2) in autosomal recessive brachyolmia (32). A direct relationship may exist between the TGF-beta signaling pathway and the *TRPV4* and *PAPSS2* genes. TRPV4 regulates cardiac fibroblast differentiation to myofibroblasts by integrating signals from TGF-beta1 and mechanical factors (33). Altered responsiveness to TGF-beta results in reduced *Papss2* expression and alterations in the biomechanical properties of mouse articular cartilage (34).

The role of LTBP3 in bone development is also exemplified by the *Ltbp3*$^{-/-}$ knockout mouse phenotype (7,8,35,36). These animals show growth retardation, obliteration of the skull synchondrosis within 2 weeks of birth, osteopetrosis of long bones and vertebrae and osteoarthritis. Thoracic kyphosis (curvature of the cervical and thoracic vertebrae) and distorted ribcage were also observed in the mutant mice. The high bone mass was related to a defect in bone resorption with compromised osteoclast function and decreased bone turnover (9). Platyspondyly however was not observed in the *Ltbp3*$^{-/-}$ knockout mice.

A wider phenotype

A previous report has described expression of *LTBP3* in various human tissues and cell lines, predominantly in heart, skeletal muscle, prostate and ovaries, as well as testis and small intestine (14). *Ltbp3* was also found to be expressed in the rat brain, with a partially overlapping expression with several other TGF-beta family members (37). Basioccipital-basisphenoid synchondrosis of P1 mouse expressed *Ltbp3* in prehypertrophic chondrocytes. *Ltbp3* transcripts were also present in adult mouse tissues in heart, brain, lung and kidney (7,8). We also report the transcription of l*tbp3* in brain vesicles, in cells surrounding the lumen of the neural tube, in the developing inner ear, in the small and large intestine, in the differentiating lung, in heart outflow tract and in the wall of the large blood vessels (Fig. 3).

It is surprising that the mutations of *LTBP3* in human seem to affect only two organ systems, the skeleton and the teeth. It will be very important to follow over time the cohort of patients to assess the clinical relevance of this *in situ* hybridization data and to record any additional occurring illness that may extent the phenotype spectrum.

Ltbp3$^{-/-}$ knockout mouse model display an enamel phenotype

Analyzing further the *Ltbp3*$^{-/-}$ knockout mouse with respect to the craniofacial and orodental phenotypes was of importance to convince that *LTBP3* is indeed the causative gene behind brachyolmia associated with AI.

As described in refs. (7–9) craniofacial malformations were identified in *Ltbp3*$^{-/-}$ mice at postnatal day 12. By 3 months of age mutant mice displayed a pronounced rounding of the cranial vault, extension of the mandible beyond the maxilla and kyphosis. The altered skull shape with occipital bossing was believed to be caused by the premature ossification of the cranial base synchondroses. Shortened skull base and disproportionately short upper jaw were evident. The external facial appearance was characterized by a rounded head and a shortened snout. Our analysis indicated that almost all craniofacial structures were affected in the *Ltbp3-null* mice. Alterations were observed in intramembranous and endochondral bones, along with in teeth. Compared with wild-type (WT) mice, *Ltbp3*-null mutants presented with an overall reduction in craniofacial size and modifications of the shape of various parts of the craniofacial skeleton. Modifications of viscerocranium, neurocranium and mandible were prominent changes.

Some of the skeletal and growth anomalies observed in the Ltbp3$^{-/-}$ mice were also present in our patients (short maxilla, mandibular prognathism) but others (such as the increased bone density) were not present, underscoring the fact that the mouse phenotype is not always recapitulating the human phenotype. We do know secreting ameloblasts express Ltbp3. The enamel was clearly defective in the mouse mutant. It was thinner, less mineralized and exhibited an unusual wavy pattern with alternating area of presence/absence. Both incisors and molars were affected. *Ltbp3*$^{-/-}$ ameloblasts as seen on histological sections of continuously growing incisor enamel organ were, in spotted area, able to synthesize an extruding NPE matrix confirming at the cellular level the impaired amelogenesis and the wavy pattern appearance.

This knockout-mice is now to be inscribed in the list of animal models presenting with enamel defects (38) and will likely serve as an important model to study further brachyolmia with AI (39).

In conclusion, the study of four unrelated families with the association of AI and brachyolmia has led to the identification of *LTBP3* as causal gene. Our study not only confirms the existence of this rare, autosomal recessive disorder but also highlights the role of *LTBP3* and TGF-beta signaling in amelogenesis, both in humans and mice. It also adds another member to the growing list of genes causing isolated and syndromic forms of brachyolmia. Study of additional families is warranted for better understanding of the phenotypic spectrum of this disorder given the wide expression of the *LTBP3* gene.

Materials and Methods

Patients

In Family 1, two sisters born from a consanguineous family of Turkish origin were referred to the Reference Center for Rare Orodental Diseases at the Strasbourg University Hospital because of pain and enamel defects (Fig. 1). Besides short stature (140 cm adult height, −4.2 SD), they also showed facial dysmorphism with large forehead, thick eyebrows, almond shaped eyes,

myopia and mild learning difficulties. Radiographs of the skeleton revealed brachyolmia (Fig. 1E and F) and there were no signs of a generalized skeletal dysplasia. Bone age was considered as normal.

Their orodental findings were documented using the D[4]/phenodent Diagnosing Dental Defects Database registry (www.phenodent.org).

Enamel was almost absent (hypoplastic AI) in both primary and permanent dentitions (Fig. 1A and B). The teeth were yellow, small and spaced. Several teeth were surgically extracted because of recurrent infections. On orthopantomogram, no enamel was observed, pulp chambers were large and molars were taurodontic (Fig. 1C). Lateral cephalogram showed somewhat thickened cortical plates of the frontal bone and an absence of pneumatization of the frontal and sphenoid sinuses. Posterior clinoid apophyses of the sphenoid were abnormally shaped. Class III mandibular prognathism was due to maxillary underdevelopment (Fig. 1D).

Family 2 consisted of two sibs born to non-consanguineous, unrelated Caucasian parents. The female proband (III.6) is the sixth child. Birth weight was 2.760 g, birth length 46 cm and head circumference was 33 cm at 39 weeks of gestation. She had normal psychomotor development and no general health problems. Primary teeth were small and yellowish with a poor square morphology and rounded cusps without pronounced fissures. The enamel was smooth and showed external crown resorption before molars erupted. She suffered of repeated dental abscesses, leading to the extraction of several teeth at ages 2½ and 5 years. When seen at age 8, she had clearly hypoplasic AI, microdontia and taurodontism. At age 13, she was 149 cm tall (−1.5 SD), weighed 42 kg and had an occipital-frontal circumference of 51 cm. She had a triangular face with retraction of the midface. She had short hands with stubby interphalangeal joints. Pro- and supination movements were limited. Osteotendinous reflexes in the lower limbs were jerky. Single nucleotide polymorphism (SNP)-array was normal (Illumina CytoSNP-12 v2) and did not reveal homozygosity stretches. Radiographs showed mild platyspondyly. Her brother (III.7) was the seventh sib of the family. He was prematurely born at 28 weeks of gestation and remained in the intensive neonatal care unit for 3 months, without major cardiopulmonary or neurological complication. Inguinal herniae were surgically corrected. He walked at age 14 months and his first words were delayed to 2½ years. He required speech therapy. When examined at age 5½ year-old, he was 101 cm tall (−3 SD), weighed 16 kg and had a head circumference of 48.5 cm. His teeth were small and yellow lacking enamel. He had a triangular face, converging squint, a narrow thorax with prominent sternum and hypermobile small joints. The family history was unremarkable. Parents had normal height (175 cm for the father and 170 for the mother) and teeth. The six other sibs were normal.

Family 3 has been described previously by Bertola *et al.* (4). The proband is a 12-year-old boy from consanguineous and healthy parents. The patient sat unsupported at 8 months of age, walked at 12 months, said his first words at 2 years. Although the mother refers some difficulties in learning, he attends a regular school (currently last year of high school). He presented with short stature (height at −3 SD for age) and enamel defects in the primary and permanent dentition. A panoramic radiograph revealed taurodontic pulp chambers of the permanent teeth. Skeletal survey showed mild flattening of the vertebral bodies with minimal posterior scalloping and no evidence of a generalized epi- or metaphyseal dysplasia. Mother and father have normal height (145 and 162.5 cm, respectively) and dental status. This was confirmed by clinical and X-ray examinations.

Family 4 includes three affected sibs in a sibship of five children born to first cousin parents of Pakistani origin. The three affected children, two girls and one boy of, respectively, 16, 9 and 12 years of age, presented with short stature (height ranging from −2 to −5 SD). They were disproportionate with short trunk due to a generalized platyspondyly. Radiographs showed osteopenia and mild vertebral flattening with posterior scalloping and superior and inferior indentations in the posterior third of the lumbar vertebrae. The oldest girl underwent surgery for an S-shaped scoliosis. The scoliosis in the two other children was rather mild. Recurrent dental abscesses were noted and the dental practitioner confirmed a diagnosis of AI with missing teeth.

None of the family members had intellectual disability. The father's height was 165.2 cm (3rd–10th centile), and the mother's height was 149.4 cm (>3rd centile). None of the unaffected member of the family have skeletal nor dental anomalies.

Genetic analyses

This study was approved by the ethics committee of the Strasbourg University Hospital (ClinicalTrials.gov Identifier: NCT01746121). Informed consent and DNA samples were obtained from all participating individuals. Genomic DNA was isolated either from blood using the Flexigene DNA kit (Qiagen, Courtaboeuf, France) or from saliva using the prepIT-L2P OG-250 Oragene®DNA kit (DNA Genotek Inc., ON, Canada). Whole-exome sequencing was performed by IntegraGen (Evry, France). The coding parts of the genome were captured using the SureSelect Human All Exon Kits V5+UTR 70 Mb (Agilent, Massy, France) and the resulting libraries were sequenced as paired-end 75 base pair reads on a HiSeq 2000 (Illumina, San Diego, USA). Image analysis and base calling were performed using the Real Time Analysis (RTA) Pipeline version 1.9 with default parameters (Illumina). The bioinformatic analysis of sequencing data was based on the CASAVA1.8 pipeline (Illumina). CASAVA performs alignment and detects variants (SNPs and indels) based on the allele calls and read depth. The variants were annotated and prioritized using an in-house pipeline VaRank (http://lbgi.fr/VaRank/, (40) (41).

Sanger sequencing (GATC Biotech, Applied Biosystems ABI 3730xl™, Konstanz, Germany) was used to validate the mutations and verify segregation using the primers shown in Supplementary Material, Table S2.

Homozygosity mapping via GeneChip Human 250 K SNP Affymetrix was performed as previously described (42) in family 1 on affected individuals IV.1, IV.2, on the unaffected individual IV.3 and both parents III.3 and III.4 (Supplementary Material, Fig. S1).

cDNA analysis

RNA was extracted from fibroblasts of patient IV.1 (gingival biopsy) and one unrelated control by using a RiboPure™ Kit, followed by a DNAse treatment with the TURBO DNA-free™ Kit (Life Technologies, Carlsbad, CA). RNA integrity was assessed by gel electrophoresis and RNA concentration was measured with the Eppendorf Biophotometer Plus™ with the Hellma® TrayCell™ (Eppendorf, Hamburg, Germany). Reverse transcription of 1 µg total RNA to cDNA was performed using the iScript™ cDNA Synthesis Kit (BioRad, Hercules, CA). Reverse transcription polymerase chain reaction was performed to determine the exon content of the cDNA from the patient. Primers used for reverse transcription polymerase chain reaction are shown in Supplementary Material, Table S2.

Scanning electron microscopy

The permanent left upper second premolar (25) of patient IV2, family 1, as well as an identical control tooth, were available for the comparative study of enamel AI/control ultrastructure. After extraction, the teeth were rinsed with tap water and immersed in a sodium hypochlorite solution (1.2 chlorometric degree) for 24 h. After a rinsing with distilled water the tooth was dehydrated in a graded series of ethanol, transferred in a solution of propylene oxide/epon resin (v/v) for 24 h, then embedded in Epon 812 (Euromedex, Souffelweyersheim, France). The tooth was sectioned into two halves along its vertical axis using a water-cooled diamond circular saw (Bronwill, NY, USA) and both surfaces were polished with diamond paste (Escil, Chassieu, France). One half was then etched with a 20% (m/v) citric acid solution for 2 min, rinsed with distilled water, dehydrated in a graded series of ethanol solutions and finally left to dry at room temperature. The samples were coated with a gold–palladium alloy using a HUMMER JR sputtering device (Technics, CA, USA). Scanning electron microscope assessments and microanalysis (Energy dispersive X-ray) were performed with a XL SIRION 200 FEG SEM (FEI company, Eindhoven, The Netherlands) operating with an electron accelerating voltage of 5 kV.

In situ hybridization

Sample preparation

Mouse embryos/fetuses were collected at E12.5, E14.5, E16.5 and E18.5, after natural mating between C57BL6 mice. All experiments were carried out in accordance with the European Community Council Directive of 24 November 1986 (86/609/EEC). The project was approved by the ICS/IGBMC animal experimentation ethics committee (2012-097). For E14.5 and older samples, the whole body was embedded in OCT 4583 medium (Tissue-TEK, Sakura) and frozen on the surface of dry ice. E12.5 embryos were fixed overnight in 4% paraformaldehyde (pH 7.5, w/v) in phosphate buffered saline (PBS), cryoprotected by overnight incubation in 20% sucrose (w/v) in PBS and cryoembedded as described above. Cryosections (Leica CM3050S cryostat) at 10 µm were collected on Superfrost plus slides and stored at −80°C until hybridization. E12.5 and E14.5 samples were sectioned in a frontal plane, whereas other stages were sectioned sagitally.

Probe synthesis

The Ltbp3 probe was synthesized from PCR-generated DNA templates kindly provided by the EURExpress consortium (http://www.eurexpress.org). The template sequence is given in Supplementary Material, Fig. S3. DIG-labeled antisense riboprobe was transcribed *in vitro* by incubation for 2 h at 37°C using 1 µg of the PCR product, 20 U SP6 RNA polymerase, 5× transcription buffer (Promega), 10× DIG RNA labeling Mix (Roche), 0.5 M 1,4-Dithiothreitol, 20 U RNAse inhibitor (Roche) in a 20-µl volume. The reaction was stopped with 2 µl EDTA (0.2 M, pH 8), and RNA was precipitated with 1 µl yeast tRNA (10 mg/ml), 2.5 µl LiCl (4 M) and 75 µl absolute ethanol, followed by an incubation for 30 min at −80°C and centrifugation at 12 000 rpm (30 min at 4°C). The pellet was washed with 0.5 ml ethanol (70%) and re-centrifuged. The supernatant was discarded and the pellet was allowed to dry. The probe was then diluted in 20 µl sterile H_2O. The quality of the probe was verified by electrophoresis in a 1% agarose gel. If no smear was observed and the size was as expected, the probe was considered to be ready for use. The quantity of RNA was evaluated by Nanodrop (ND-1000 Spectrophotometer, Labtech) and adjusted to 150 ng/µl in hybridization buffer, then stored at −20°C until use.

In situ hybridization

In situ hybridization was performed as previously described (43).

MicroCT imaging

Fixed in ethanol heads of 7 (5 × 3.5 months-old and 2 × 5.5 months-old) mutant *Ltbp3*$^{-/-}$ mice and 7 WT littermates were analyzed through X-ray micro-CT using Quantum FX® microCT Pre-clinical In Vivo Imaging System (Caliper Life Sciences, Inc., Hopkinton, MA, USA), which operates at an energy of 80 kV and current intensity of 160 µA, with high-resolution detection at 10–295 µm pixel size. 3D data reconstructions were performed using Analyze software (v 11.0; Biomedical Imaging Resource, Mayo Clinic, Rochester, MN). Animals necropsy material was kindly provided by B. Dabovic and D.B. Rifkin, Department of Cell Biology, NYU Langone Medical Center, New York, NY.

Histological analysis

Fixed in 10% formalin and then transferred in 70% ethanol, heads of 3.5 months-old WT and *Ltbp3*$^{-/-}$ mice were washed in water and then demineralized in EDTA 10% in H_2O at 37°C for 10 days (the demineralizing solution was changed every day for the first 3 days and then every other day). After thorough water washes, the heads were dehydrated in graded ethanol, cleared in histosol and embedded in paraffin at 60°C. 10 µm transversal sections were stained with hematoxylin/eosin. A detailed histology protocol can be found at http://www.empress.har.mrc.ac.uk.

Supplementary Material

Supplementary Material is available at *HMG* online.

Acknowledgements

We would like to thank the patients and families for their participation. We are grateful to Nadia Messaddeq from the IGBMC Imaging centre for her help and support and to Yann Hérault and Isabelle Goncalves da Cruz from the Mouse Clinical Institute for facilitating access to the Micro-CT imaging. We thank Vanessa Stoehr for her efficient management of the INTERREG project. All contributors have read and approved the submitted manuscript.

Conflict of Interest statement. None declared.

Funding

This work was supported by grants from the University of Strasbourg, the French Ministry of Health (National Program for Clinical Research, PHRC 2008 No. 4266 Amelogenesis imperfecta), the Hôpitaux Universitaires de Strasbourg (API, 2009-2012, 'Development of the oral cavity: from gene to clinical phenotype in Human'), IFRO (Institut Français pour la Recherche Odontologique) and the EU-funded project (ERDF) A27 'Oro-dental manifestations of rare diseases', supported by the RMT-TMO Offensive Sciences initiative, INTERREG IV Upper Rhine program www.genosmile.eu. Work performed at IGBMC was supported by the grant ANR-10-LABX-0030-INRT, a French State fund managed by the Agence Nationale de la Recherche under the frame programme Investissements d'Avenir labelled ANR-10-IDEX-0002-02. Funding was also received under the European Commission Seventh

Framework Programme (SYBIL project; grant number 602300). E.B. holds a post-doctoral fellowship of the FWO (Fund for Scientific Research—Flanders). B.B.D. and D.BR. are funded by National Institutes of Health: NIH R01 CA034282. Funding to pay the Open Access publication charges for this article was provided by the EU-funded project (ERDF) A27 "Oro-dental manifestations of rare diseases", supported by the RMT-TMO Offensive Sciences initiative, INTERREG IV Upper Rhine program www.genosmile.eu.

Web Resources

The URLs for data presented herein are as follows:
1000 Genome Browser, http://browser.1000genomes.org
BDGP, http://www.fruitfly.org
D[4]/phenodent Diagnosing Dental Defects Database, www.phenodent.org
dbSNP, http://www.ncbi.nlm.nih.gov/projects/SNP
Ensembl Genome Browser, http://www.ensembl.org
Eurexpress, http://www.eurexpress.org/ee/
Exome Variant Server (EVS) http://evs.gs.washington.edu/EVS/
GenBank, http://www.ncbi.nlm.nih.gov/Genbank
GeneHub-GEPIS, http://www.cgl.ucsf.edu/Research/genentech/genehub-gepis/genehubgepis-search.html
Gene expression in tooth, http://bite-it.helsinki.fi
GenePaint, http://www.genepaint.org
HSF2.4.1, http://www.umd.be/HSF
NCBI, http://www.ncbi.nlm.nih.gov/
Online Mendelian Inheritance in Man (OMIM), http://www.omim.org
UCSC Genome Browser, http://genome.ucsc.edu/cgi-bin/hgGateway
UniGene, http://www.ncbi.nlm.nih.gov/unigene
VaRank, http://lbgi.fr/VaRank/
EMBL-EBI Interpro, http://www.ebi.ac.uk/interpro/
EMPReSS, http://www.empress.har.mrc.ac.uk

References

1. Crawford, P.J., Aldred, M. and Bloch-Zupan, A. (2007) Amelogenesis imperfecta. *Orphanet J. Rare Dis.*, **2**, 17.
2. Bloch-Zupan, A., Sedano, H. and Scully, C. (2012) *Dento/Oro/Craniofacial Anomalies and Genetics*. Elsevier Inc., London.
3. Verloes, A., Jamblin, P., Koulischer, L. and Bourguignon, J.P. (1996) A new form of skeletal dysplasia with amelogenesis imperfecta and platyspondyly. *Clin. Genet.*, **49**, 2–5.
4. Bertola, D.R., Antequera, R., Rodovalho, M.J., Honjo, R.S., Albano, L.M., Furquim, I.M., Oliveira, L.A. and Kim, C.A. (2009) Brachyolmia with amelogenesis imperfecta: further evidence of a distinct entity. *Am. J. Med. Genet. A*, **149A**, 532–534.
5. Noor, A., Windpassinger, C., Vitcu, I., Orlic, M., Rafiq, M.A., Khalid, M., Malik, M.N., Ayub, M., Alman, B. and Vincent, J.B. (2009) Oligodontia is caused by mutation in LTBP3, the gene encoding latent TGF-beta binding protein 3. *Am. J. Hum. Genet.*, **84**, 519–523.
6. Laugel-Haushalter, V., Paschaki, M., Thibault-Carpentier, C., Dembele, D., Dolle, P. and Bloch-Zupan, A. (2013) Molars and incisors: show your microarray IDs. *BMC Res. Notes*, **6**, 113.
7. Dabovic, B., Chen, Y., Colarossi, C., Zambuto, L., Obata, H. and Rifkin, D.B. (2002) Bone defects in latent TGF-beta binding protein (Ltbp)-3 null mice; a role for Ltbp in TGF-beta presentation. *J. Endocrinol.*, **175**, 129–141.
8. Dabovic, B., Chen, Y., Colarossi, C., Obata, H., Zambuto, L., Perle, M.A. and Rifkin, D.B. (2002) Bone abnormalities in latent TGF-[beta] binding protein (Ltbp)-3-null mice indicate a role for Ltbp-3 in modulating TGF-[beta] bioavailability. *J. Cell Biol.*, **156**, 227–232.
9. Dabovic, B., Levasseur, R., Zambuto, L., Chen, Y., Karsenty, G. and Rifkin, D.B. (2005) Osteopetrosis-like phenotype in latent TGF-beta binding protein 3 deficient mice. *Bone*, **37**, 25–31.
10. Nieman, B.J., Wong, M.D. and Henkelman, R.M. (2011) Genes into geometry: imaging for mouse development in 3D. *Curr. Opin. Genet. Dev.*, **21**, 638–646.
11. Klopcic, B., Maass, T., Meyer, E., Lehr, H.A., Metzger, D., Chambon, P., Mann, A. and Blessing, M. (2007) TGF-beta superfamily signaling is essential for tooth and hair morphogenesis and differentiation. *Eur. J. Cell Biol.*, **86**, 781–799.
12. Annes, J.P., Munger, J.S. and Rifkin, D.B. (2003) Making sense of latent TGFbeta activation. *J. Cell Sci.*, **116**, 217–224.
13. Hyytiainen, M., Penttinen, C. and Keski-Oja, J. (2004) Latent TGF-beta binding proteins: extracellular matrix association and roles in TGF-beta activation. *Crit. Rev. Clin. Lab. Sci.*, **41**, 233–264.
14. Penttinen, C., Saharinen, J., Weikkolainen, K., Hyytiainen, M. and Keski-Oja, J. (2002) Secretion of human latent TGF-beta-binding protein-3 (LTBP-3) is dependent on co-expression of TGF-beta. *J. Cell Sci.*, **115**, 3457–3468.
15. Inage, T., Fujita, M., Kobayashi, M., Wakao, K., Saito, N., Shibuya, H., Shimada, M. and Takagi, K. (1990) Ultrastructural differentiation in the distal ends of ameloblasts from the presecretory zone to the early secretory zone. *J. Nihon Univ. Sch. Dent.*, **32**, 259–269.
16. Zhu, Q., Fan, M., Bian, Z., Chen, Z., Zhang, Q. and Peng, B. (2000) In situ hybridization analysis of transforming growth factor-beta 1 RNA expression during mouse tooth development. *Chin. J. Dent. Res.*, **3**, 21–25.
17. Fan, M.W., Bian, Z. and Gao, Y.G. (1998) Immunohistochemistry and in situ hybridization investigation of transforming growth factor-beta: during odontoblast and ameloblast differentiation. *Chin. J. Dent. Res.*, **1**, 17–21.
18. Khan, Q.E., Sehic, A., Khuu, C., Risnes, S. and Osmundsen, H. (2013) Expression of Clu and Tgfb1 during murine tooth development: effects of in-vivo transfection with anti-miR-214. *Eur. J. Oral Sci.*, **121**, 303–312.
19. Haruyama, N., Thyagarajan, T., Skobe, Z., Wright, J.T., Septier, D., Sreenath, T.L., Goldberg, M. and Kulkarni, A.B. (2006) Overexpression of transforming growth factor-beta1 in teeth results in detachment of ameloblasts and enamel defects. *Eur. J. Oral Sci.*, **114**(Suppl 1), 30–34.
20. Gao, Y., Li, D., Han, T., Sun, Y. and Zhang, J. (2009) TGF-beta1 and TGFBR1 are expressed in ameloblasts and promote MMP20 expression. *Anat. Rec. (Hoboken)*, **292**, 885–890.
21. Tsuchiya, M., Sharma, R., Tye, C.E., Sugiyama, T. and Bartlett, J.D. (2009) Transforming growth factor-beta1 expression is up-regulated in maturation-stage enamel organ and may induce ameloblast apoptosis. *Eur. J. Oral Sci*, **117**, 105–112.
22. Suzuki, M., Shin, M., Simmer, J.P. and Bartlett, J.D. (2014) Fluoride Affects Enamel Protein Content via TGF-beta1-mediated KLK4 Inhibition. *J. Dent. Res.*, **93**, 1022–1027.
23. Cho, A., Haruyama, N., Hall, B., Danton, M.J., Zhang, L., Arany, P., Mooney, D.J., Harichane, Y., Goldberg, M., Gibson, C.W. *et al.* (2013) TGF-ss regulates enamel mineralization and maturation through KLK4 expression. *PLoS One*, **8**, e82267.
24. Tjaderhane, L., Koivumaki, S., Paakkonen, V., Ilvesaro, J., Soini, Y., Salo, T., Metsikko, K. and Tuukkanen, J. (2013) Polarity of mature human odontoblasts. *J. Dent. Res.*, **92**, 1011–1016.
25. Sehic, A., Risnes, S., Khan, Q.E., Khuu, C. and Osmundsen, H. (2010) Gene expression and dental enamel structure in developing mouse incisor. *Eur. J. Oral Sci.*, **118**, 118–130.
26. Lacruz, R.S., Nakayama, Y., Holcroft, J., Nguyen, V., Somogyi-Ganss, E., Snead, M.L., White, S.N., Paine, M.L. and Ganss, B.

(2012) Targeted overexpression of amelotin disrupts the microstructure of dental enamel. *PLoS One*, **7**, e35200.
27. Bartlett, J.D. and Simmer, J.P. (2014) Kallikrein-related peptidase-4 (KLK4): role in enamel formation and revelations from ablated mice. *Front. Physiol.*, **5**, 240.
28. Koli, K., Ryynanen, M.J. and Keski-Oja, J. (2008) Latent TGF-beta binding proteins (LTBPs)-1 and -3 coordinate proliferation and osteogenic differentiation of human mesenchymal stem cells. *Bone*, **43**, 679–688.
29. Kanaan, R.A. and Kanaan, L.A. (2006) Transforming growth factor beta1, bone connection. *Med. Sci. Monit.*, **12**, RA164–RA169.
30. Alliston, T., Piek, E. and Derynck, R. (2008) 22 TGF-β Family Signaling in Skeletal Development, Maintenance, and Disease. In Derynck, R. and Miyazono, K. (eds), *The TGF-Beta Family*. Cold Spring Harbor Monograph Archive, North America, 50. Available at: https://cshmonographs.org/index.php/monographs/article/view/3854 (last accessed, 17 February 2015).
31. Grigelioniene, G., Geiberger, S., Horemuzova, E., Mostrom, E., Jantti, N., Neumeyer, L., Astrom, E., Nordenskjold, M., Nordgren, A. and Makitie, O. (2014) Autosomal dominant brachyolmia in a large Swedish family: phenotypic spectrum and natural course. *Am. J. Med. Genet. A*, **164**, 1635–1641.
32. Iida, A., Simsek-Kiper, P.O., Mizumoto, S., Hoshino, T., Elcioglu, N., Horemuzova, E., Geiberger, S., Yesil, G., Kayserili, H., Utine, G.E. *et al.* (2013) Clinical and radiographic features of the autosomal recessive form of brachyolmia caused by PAPSS2 mutations. *Hum. Mutat.*, **34**, 1381–1386.
33. Adapala, R.K., Thoppil, R.J., Luther, D.J., Paruchuri, S., Meszaros, J.G., Chilian, W.M. and Thodeti, C.K. (2013) TRPV4 channels mediate cardiac fibroblast differentiation by integrating mechanical and soluble signals. *J. Mol. Cell. Cardiol.*, **54**, 45–52.
34. Ramaswamy, G., Sohn, P., Eberhardt, A. and Serra, R. (2012) Altered responsiveness to TGF-beta results in reduced Papss2 expression and alterations in the biomechanical properties of mouse articular cartilage. *Arthritis Res. Ther.*, **14**, R49.
35. Colarossi, C., Chen, Y., Obata, H., Jurukovski, V., Fontana, L., Dabovic, B. and Rifkin, D.B. (2005) Lung alveolar septation defects in Ltbp-3-null mice. *Am. J. Pathol.*, **167**, 419–428.
36. Chen, Y., Dabovic, B., Colarossi, C., Santori, F.R., Lilic, M., Vukmanovic, S. and Rifkin, D.B. (2003) Growth retardation as well as spleen and thymus involution in latent TGF-beta binding protein (Ltbp)-3 null mice. *J. Cell. Physiol.*, **196**, 319–325.
37. Dobolyi, A. and Palkovits, M. (2008) Expression of latent transforming growth factor beta binding proteins in the rat brain. *J. Comp. Neurol.*, **507**, 1393–1408.
38. Pugach, M.K. and Gibson, C.W. (2014) Analysis of enamel development using murine model systems: approaches and limitations. *Front. Physiol.*, **5**, 313.
39. Fleischmannova, J., Matalova, E., Tucker, A.S. and Sharpe, P.T. (2008) Mouse models of tooth abnormalities. *Eur. J. Oral Sci.*, **116**, 1–10.
40. Geoffroy, V., Pizot, C., Redin, C., Piton, A., Vasli, N., Stoetzel, C., Blavier, A., Laporte, J. and Muller, J. (2015) VaRank: a simple and powerful tool for ranking genetic variants. *PeerJ*. in press.
41. Redin, C., Le Gras, S., Mhamdi, O., Geoffroy, V., Stoetzel, C., Vincent, M.C., Chiurazzi, P., Lacombe, D., Ouertani, I., Petit, F. *et al.* (2012) Targeted high-throughput sequencing for diagnosis of genetically heterogeneous diseases: efficient mutation detection in Bardet-Biedl and Alstrom syndromes. *J. Med. Genet.*, **49**, 502–512.
42. Bloch-Zupan, A., Jamet, X., Etard, C., Laugel, V., Muller, J., Geoffroy, V., Strauss, J.P., Pelletier, V., Marion, V., Poch, O. *et al.* (2011) Homozygosity mapping and candidate prioritization identify mutations, missed by whole-exome sequencing, in SMOC2, causing major dental developmental defects. *Am. J. Hum. Genet.*, **89**, 773–781.
43. Laugel-Haushalter, V., Langer, A., Marrie, J., Fraulob, V., Schuhbaur, B., Koch-Phillips, M., Dolle, P. and Bloch-Zupan, A. (2012) From the transcription of genes involved in ectodermal dysplasias to the understanding of associated dental anomalies. *Mol. Syndromol.*, **3**, 158–168.